


Detailed precision and accuracy analysis of swarm parameters from a pulsed Townsend experiment

Journal Article**Author(s):**

Haefliger, Pascal; [Franck, Christian](#) 

Publication date:

2018-02-23

Permanent link:

<https://doi.org/10.3929/ethz-b-000248781>

Rights / license:

[In Copyright - Non-Commercial Use Permitted](#)

Originally published in:

Review of Scientific Instruments 89(2), <https://doi.org/10.1063/1.5002762>

This is a pre-refereeing copy of the manuscript
submitted to AIP (Author's original)

This is an author-created, un-copyedited version of an article
published in Journal of Physics D: Applied Physics. IOP Publishing
Ltd is not responsible for any errors or omissions in this version of the
manuscript or any version derived from it. The Version of Record is
available online at <https://doi.org/10.1063/1.5002762>

Detailed precision and accuracy analysis of swarm parameters from a Pulsed Townsend experiment

P. Haefliger¹, C. M. Franck¹

¹Power Systems and High Voltage Laboratories, ETH Zurich, Physikstr. 3, 8092 Zurich, Switzerland

E-mail: hapascal@ethz.ch

February 2017

Abstract. A newly built Pulsed Townsend experimental setup which allows to measure both electron and ion currents is presented. Based on findings operating a previous experiment and on literature, the accuracy of the experimental input parameters was identified as necessary requirement to obtain accurate swarm parameters such as the effective ionization rate coefficient, the density-reduced mobility and the density-normalized longitudinal diffusion coefficient. The influence of the input parameters (gap distance, applied voltage, measured pressure and temperature) is analyzed in detail. An overall accuracy of $\pm 0.5\%$ in the density reduced electric field (E/N) is achieved, which is close to the theoretically possible limit using the chosen components. The precision of the experimental results is higher than the accuracy. Through an extensive measurement campaign, the repeatability of our measurements proved to be high and similar to the precision. The reproducibility of results at identical (E/N) is similar to the precision for different distances but decreases for varying pressures. For benchmark purposes, measurements for Ar, CO₂ and N₂ are presented and compared with our previous experimental setup, simulations and other experimental references.

PACS numbers: 00.00, 20.00, 42.10

Submitted to: *Rev. Sci. Instrum.*

Definitions (from [1] based on GUM [2]):

True value:	Value that would be obtained by a perfect measurement, true values are indeterminate by nature.
Accuracy:	Closeness of the agreement between the result of a measurement and a true value of the measurand.
Error:	Difference between a measurement and the true value of the measurand.
Precision:	Closeness of agreement between independent measurements of a quantity under the same conditions. It is a measure of how well a measurement can be made without reference to a theoretical or true value (only in [1]). For example the ionization rate is determined by a linear regression of the $\log(I)$ versus time there a random noise affecting I would affect the obtained ionization rate. I is the measured current.
Repeatability:	Precision of results of successive, independent measurements carried out under the same conditions.
Reproducibility:	Precision of results of successive independent measurements carried out under different conditions.
Uncertainty:	Parameter, associated with the result of a measurement, that characterizes the dispersion of the values that could reasonably be attributed to the measurand.

1. Introduction

Swarm experiments are used to measure the electron and ion transport properties in gases, which are required to understand and predict their behavior in various applications such as: pollution control [3], etching gases [4], biomedical applications such as microdosimetry [5] or particle detectors such as resistive plate chambers [6]. Besides these applications we are interested in using gases as electrical insulators [7]. To measure the swarm parameters we use a Pulsed Townsend (PT) experiment. With this experiment and applied evaluation methods swarm parameters are obtained. The swarm parameters are a function of the reduced electric field (E/N).

To obtain swarm parameters with high accuracy, it is most important to precisely know (E/N). The electrical field E is obtained by the electrode separation distance d and the applied voltage U . N is the gas density (number of molecules per m^3) which results from the pressure p and temperature T in the chamber applying the ideal gas law. The best example to illustrate the necessity of a highly precise (E/N)-value is the ionization rate coefficient, which increases almost exponentially with (E/N). Such a detailed analysis of the precision, error, repeatability and reproducibility has not been conducted before, to the best of the author's knowledge. Nevertheless, these are essential to increase the

comparability of different experiments.

Based on the experience of using a previous experimental setup [8] for several years and on descriptions of other PT experiments [9, 10, 11, 12], an improved PT setup was built. In section 2 the new setup is described, section 3 outlines the analytical model, section 4 explains the results of Ar, N₂ and CO₂ with emphasis on the accuracy, and in section 5 the design and the accuracy of the PT experiment are discussed. The error analysis and benchmark measurements presented in this contribution rely on measurements of the explained setup.

2. Experiment

The advantage of the new setup compared to the previous one [8] are an improved electrode support which guarantees a pressure independent and precise gap distance, higher electric field homogeneity, and a gate valve which brings ease in gas handling. The actuators and sensors control remained unchanged. As the accuracy of the used components is given by the manufacturer, the aim was to construct an electrode support accurate enough to achieve an overall accuracy in (E/N) of $\pm 0.5\%$.

2.1. Setup of PT experiment

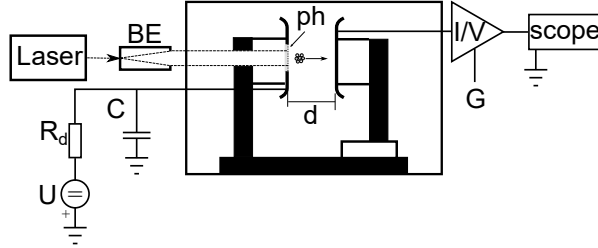
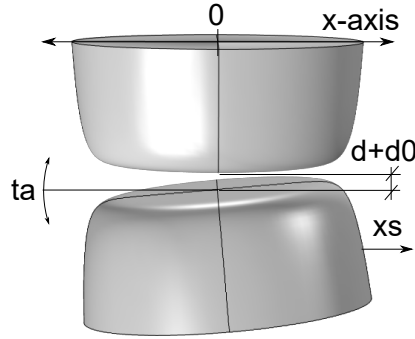


Figure 1: Two electrodes with a gap distance d are mounted inside a vacuum chamber. On the cathode side an HV-source (with a DC-supply voltage U) is connected. R_d and C decouple the HV-source from the signal circuit. A UV-laser beam, which is broadened through a beam expander (BE), releases electrons from the photocathode (ph). The electrons and ions drift in the electric field between the electrodes. A displacement current is measured on the anode side with a transimpedance amplifier of variable gain G and a scope [13].

The experimental parts are housed inside a stainless steel vessel with a diameter and length of 50 cm each, resulting in a volume of about 100l. Connected gas equipment is chosen to deal with gas purities class 5 (99.999% purity) and 6. The vessel base pressure is around 10^{-6} Pa. Gas samples can be mixtures with up to three components filled in via gas flow controllers. The mixing ratio is defined by measuring the gases' partial

pressures. The gas pressures can be accurately measured in the range from 10^{-2} Pa up to 100 kPa by using three Pfeiffer Vacuum gauges of the type CMR364, CMR371 and CMR372. The CMR371 and 372 used for pressure measurements from 100 Pa to 100 kPa, have a resolution of 0.003 % full scale and an accuracy of 0.15 % of the reading and a temperature influence on the span of 0.01 % of the reading per $^{\circ}$ C. In this setup the temperature is measured with a T-Type thermocouple, which has a good thermal connection to the chamber vessel. The analog-to-digital-converter (ADC), LabJack (U6), has an input range of 100 mV and a resolution of 17bit. The accuracy of the measurement temperature is 0.01%. The lab itself has a temperature regulation of 293 ± 2 K.

(a)



(b)

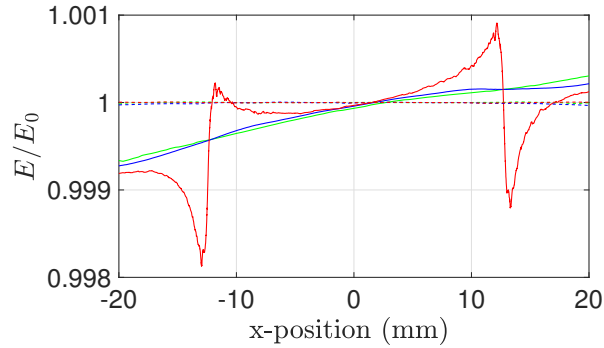


Figure 2: (a) Drawing of Rogowski electrodes which deviates from the ideal arrangement by an offset (d_0) to the wanted gap distance (d), a radial displacement (x_s) and a tilt (t_a) between the electrodes. Missing is the distortion by the photocathode. (b) The homogeneity of the electric field is analyzed with a FEM simulation in the worst case. The y-axis is the electric field normalized to a homogeneous field E_0 . The x-axis displays the area around the photocathode (diameter 25 mm) where the electron swarm is released. Compared is: (----) an ideal Rogowski-profile to the used real one at different positions (—) cathode, (—) center and (—) anode [13].

The electrode construction was optimized to control the exact electrode gap distance d , to minimize the distortion of the electric field homogeneity, to provide mechanical long term stability and high reproducibility. This was achieved by using mechanical locators [13]. To avoid that changes in pressure influence the electrode arrangement, the electrodes are mounted on a rigid steel plate decoupled from the chamber flanges or walls as depicted in fig. 1. The accuracy and repeatability of the electrode positioning is identified by a 3-D coordinate measurement device from Mitutoyo type KN815 which has a certified accuracy of $\pm 2 \mu\text{m}$. The reproducibility of the distance is within $\pm 10 \mu\text{m}$. The electrode plane tilt angle is smaller than 0.02° and the radial displacement of the electrodes is smaller than $\pm 170 \mu\text{m}$. Several measurements over a time period of over a year have confirmed the mechanical system stability and reproducibility. In the laboratory this accuracy was confirmed with gage bodies of different sizes that offer an accuracy of $\pm 5 \mu\text{m}$.

To obtain a homogeneous electric field, Rogowski-shaped electrodes designed for 15 mm gap distance are used [14]. The homogeneity of the electric field was optimized using a FEM-tool. The FEM-simulation considers the following four deviations from the ideal Rogowski-profile: the varying gap distance between 11 . . . 35 mm, the tilt angle of the electrode plates (0.02°), the radial displacement ($\pm 170 \mu\text{m}$) and the photocathode protrusion ($\pm 3 \mu\text{m}$). The resulting electric field is shown in fig. 2b. In our electrode arrangement the largest inhomogeneity contributions stem from the tilt angle and the photocathode protrusion (dominant only in front of the cathode).

Besides the mechanical construction, the electric field is also influenced by the voltage source. To reduce this error, a high precision DC voltage source is included in the setup. A DC voltage up to 60 kV is supplied and measured with a 16 bit ADC. It has a high stability and deviates less than 0.001% of 60 kV over 8h.

Oscillations, high frequency noise and recharging currents disturb the measurement signal. Similar effects have been reported in [10]. Hence, to allow a proper signal evaluation, it is necessary to install a damping resistor $R_d = 1 \text{ M}\Omega$ and a parallel stabilization capacitor $C = 2 \text{ nF}$ on the high voltage side.

A photocathode is used as the electron source. It is a quartz window coated with a thin metal film, single or double layers [15]. Materials of choice are palladium for single layer and copper-palladium or magnesium-palladium for double layers. These materials proved to have a high quantum efficiency for a large number of experiments. In the presented measurements a palladium cathode was used. To release electrons from the photocathode metal film, a pulsed laser from Crylas, type FQSS 266-200 is used. The laser wavelength is 266 nm, the pulse width (FWHM) is 1.5 ns with an energy of $200 \mu\text{J}$ per pulse and a repetition rate of 20 Hz. The beam diameter is 0.8 mm, which is widened with a 10x UV-beam expander to increase the illuminated area on the photocathode.

The measured current signal is coupled out from the vacuum vessel via a high performance microwave cable from Huber+Suhner suitable for vacuum environments, which has a capacitance of 26 pF. To amplify the signal we use a FEMTO DHPA-100 trans-impedance amplifier with variable gain G . The amplifier bandwidth depends on the gain and the source capacitance. For electron currents an amplification of 10^3 with an ideal bandwidth of 175 MHz at 10 pF source capacitance is chosen. The calculated capacitance values for our setup and electrode configuration varies (depending on the gap distance) between 34 pF and 44 pF, which reduces the bandwidth to 70-80 MHz according to the manufacturers data sheet. The measured currents are recorded by a R&S RTE scope. Its bandwidth is 2 GHz and it records 5 GS/s. The ADC has a 8 bit resolution and the waveform averaging is done on a math channel. The trigger signal is received from the laser photo diode.

2.2. Operation procedure and range

Paschen-law implies that at fixed (E/N) , the swarm parameters are fixed [16], if the gas shows no pressure-dependence. Accordingly, the measurements are performed in an automatized loop for the same (E/N) at different pressures (from 2-100 kPa), distances (from 11-35 mm) and the corresponding voltages (from 0-60 kV). After checking the limits of (U, d, p) , no user interaction is needed. The number of released start electrons is regulated between 10-20 million electrons per pulse using an attenuator.

3. Evaluation method

Two methods are available to evaluate the measured electron and ion currents. A simple method which can be used to analyze solely electron currents or electron and ion currents together is described in [17]. It includes one electron attachment and one ionization process, hence one species of positive and negative ions. It is possible to fit the measured current to an analytical formula. The present measurements are evaluated with this method. In fig.3 an evaluated electron and ion current waveform in CO_2 are presented. If processes such as detachment, ion conversion occur, a more complex method is used [18].

3.1. Electron and ion current model

All the charge carriers such as electrons, positive and negative ions contribute to the total measured current. Electron and ion drift velocities typically differ by three orders of magnitude. Therefore, they are obtained by two measurements on different timescales as shown in fig. 3. Eq. (1) [17] describes the electron current $I_e(t)$ due to the motion of electrons in the electrode gap. At instant T_0 the laser releases n_0 electrons from the photocathode with the elementary charge q_0 resulting in the measured current amplitude I_0 . The electrons form a spatially Gaussian distributed swarm. This swarm drifts with the electron drift velocity w_e in the gap d where the voltage U is applied and arrives

at instant T_e . During the electron drift, the swarm broadens with the characteristic time for longitudinal electron diffusion τ_d . The number of electrons in the gap changes according to the effective ionization rate ν_{eff} . At T_e the electrons arrive at the anode. The absorption of electrons in eq. (1) is modeled by the error function (erf). All the mentioned time instants are illustrated in fig. 3a. The effective ionization rate ν_{eff} is obtained by a linear regression of $\log(I_e)$ versus time between T_1 and T_2 . τ_d and T_e are obtained by a fit of eq. (1) between T_2 and T_3 . During the electron drift the ion current is subtracted.

$$I_e(t) = \frac{I_0}{2} \exp(\nu_{\text{eff}}(t - T_0)) \left(1 - \text{erf}\left(\frac{t - T_e}{\sqrt{2\tau_d}(t - T_0)}\right) \right) \quad (1)$$

$$I_0 = \frac{n_0 q_0}{(T_e - T_0)} \quad (2)$$

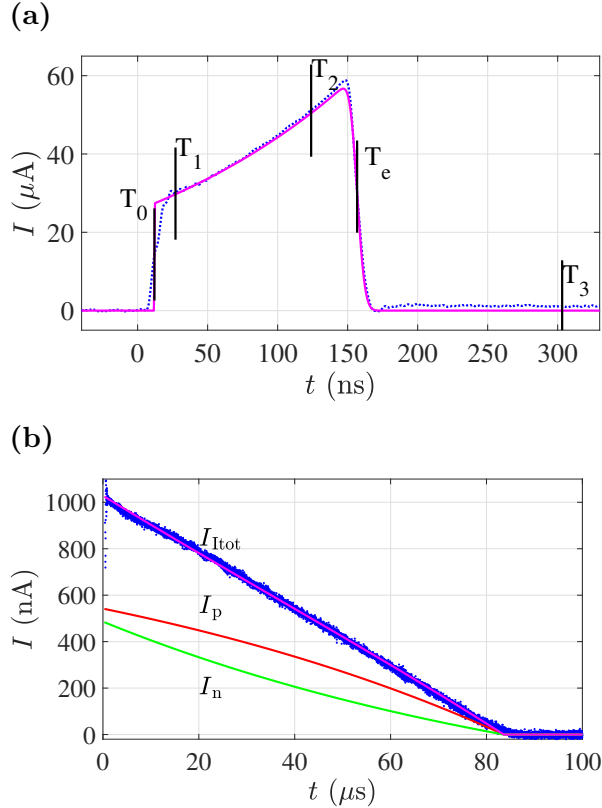


Figure 3: Measured current vs. time averaged over 150 single shots) (.....) in 60kPa CO_2 at 19mm gap distance and $(E/N) = 85 \text{ Td}$. (a) Electron current (—) fit and waveform are compared. Time marker T_{1-3} indicate fit ranges on the waveform. (b) The (—) total fitted ion current I_{tot} and individual contributions of (—) positive I_p and (—) negative ions I_n are compared to the measured ion current.

During the electron drift time, electrons generate positive ions with the rate ν_i and negative ions with ν_a . ν_{eff} is defined as $\nu_i - \nu_a$. After the electron drift time, the

time-dependent ion currents ($t' = t - T_e$) can be described by eqs. (4) and (5) for the positive and negative ions, respectively. The positive and negative ions drift with the velocity $w_p = d/T_p$ and $w_n = d/T_n$, respectively, whereas T_p and T_n are the drift times of positive and negative ions. The total measured ion current, shown in fig. 3b, is the sum of negative and positive ion currents eq. (3).

$$I_{\text{tot}}(t) = I_p(t) + I_n(t) \quad (3)$$

$$I_p(t') = I_0 \frac{T_e}{T_p} \frac{\nu_i}{\nu_{\text{eff}}} (\exp(\nu_{\text{eff}} T_e) - \exp(\nu_{\text{eff}} \frac{T_e}{T_p} t')) \quad (4)$$

$$I_n(t') = I_0 \frac{T_e}{T_n} \frac{\nu_a}{\nu_{\text{eff}}} (\exp(\nu_{\text{eff}} T_e (1 - \frac{t'}{T_n})) - 1) \quad (5)$$

The spatial swarm parameters, the longitudinal diffusion coefficient D_L and the effective ionization coefficient α_{eff} are obtained by using the following relations:

$$D_L = \tau_d \cdot w_e^2 \quad (6)$$

$$\alpha_{\text{eff}} = \nu_{\text{eff}} / w_e \quad (7)$$

4. Results

In this section the precision and accuracy of our experiment and results are quantified. To distinguish between precision of the evaluation method and experimental data, the evaluation method's sensitivity towards changes of the input parameters is validated. In addition, the reproducibility and repeatability of the measurements are addressed. The definitions are used according to the Guide to the Expression of Uncertainty in Measurements (GUM) [2]. To underline the claimed accuracy and precision, two different N_2 data sets derived from two measurement sequences are used. 1) A N_2 measurement sequence at the same (E/N) -value (110 Td) and $d=25\text{mm}$, is repeated for two different pressures ($p=3\text{kPa}$, 10kPa). To investigate the reproducibility of the experimental setup, the distances and voltages are altered 10 times in between each measurement. This data set is used in fig.4-7. 2) A N_2 measurement sequence with different (E/N) -values ($E/N=30-150\text{ Td}$), each (E/N) -value was remeasured with different sets of experimental input parameters (U, d, p) . Data set 2) is only presented in fig. 7. In the end of this section benchmark results of Ar, CO_2 and N_2 are visualized in fig. 8-12.

4.1. Theoretical error in (E/N) based on experimental input parameters

The theoretical uncertainty in (E/N) can be calculated with the Gaussian error propagation law eqs. (8) and (9), using the values given in section 2 and experimental parameters from data set 1). Parameters not yet introduced are the inhomogeneity of the electric field $E_{\text{inh}}=0.2\%$ (value taken from fig. 2b) and the Boltzmann constant k_B . As representative example the input parameters from 3 kPa N_2 measurements at

U	d	p	T
1.0 kV	13 mm	3.0 kPa	298.3 K
ΔU	Δd	ΔT	Δp
1.5 V	10 μm	0.08 K	6.3 Pa
ΔE_{inh}^2	ΔE	$\Delta E/N$	
160 (V/m) ²	243 V/m	0.42 Td	

Table 1: Overview of the used input parameters and results of the theoretical error calculation.

13 mm gap distance as a worst case scenario are used. Overall, the calculated theoretical error of ± 0.42 Td corresponds to an error of $\pm 0.38\%$ at 110 Td. The results and input parameters are listed in table 1.

$$\Delta E = \sqrt{\left(\frac{\Delta U}{d}\right)^2 + \left(\frac{U \cdot \Delta d}{d^2}\right)^2 + \Delta E_{inh}^2} \quad (8)$$

$$\Delta\left(\frac{E}{N}\right) = \frac{E}{N} \cdot \sqrt{\left(\frac{\Delta E}{E}\right)^2 + \left(\frac{\Delta T}{T}\right)^2 + \left(\frac{\Delta p}{p}\right)^2} \quad (9)$$

4.2. Assessing the evaluation accuracy and precision

A single measured displacement current waveform is subject to random noise, which results in a large dispersion of the evaluated swarm parameters. A common method to reduce noise is averaging. Depending on the signal to noise ratio (SNR) between 150 and 400 single waveform measurements are averaged (referenced later as waveform or average waveform). Multiple measured averaged waveforms are defined as measurement sequence.

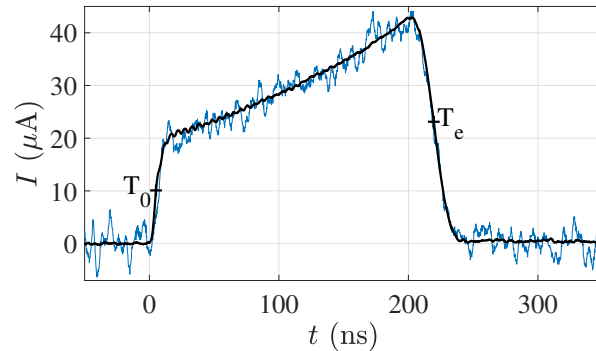


Figure 4: Measurement with typical best SNR in N_2 at $p = 10$ kPa, $d = 25$ mm and $(E/N) = 110$ Td. (—) single waveform and (—) average of 200 single waveforms. (+) T_0 and T_e of average.

Fig. 4 shows a single measurement waveform with a typical best SNR, together with an average curve from 200 single waveforms. As expected the average has a better SNR than the single waveform. The markers indicate T_0 and T_e . The average waveform rise time around T_0 (from 10 to 90%) is ~ 5.3 ns. It is not clear in detail how the rising edge of T_0 is formed. Contributions at hand are laser pulse width, amplifier bandwidth and time constant of the process to release electrons from the photocathode metal film. To demonstrate the repeatability and reproducibility of setting (E/N) , data set 1) is used. (E/N) was set newly to 110 Td, and 200 single waveforms were recorded and evaluated. Normally only average waveforms are saved for regular measurement sequences. To test for repeatability, a fixed parameter set of (U, d, p) is used in subsequent measurements. The individual results should be very close to each other. In analogy to repeatability, reproducibility is the same but with a changing set of parameters (U, d, p) . The evaluated drift times $T = T_e - T_0$ and effective ionization rates coefficients ν/N for the 9 measurement sets at $d = 25$ mm are shown for two pressures $p = 3$ kPa and $p = 10$ kPa in fig. 5. The data selection is arbitrary and can be seen as representative for the whole data set. In the boxplots, the center line is the median and the upper and lower lines mark the 75% and 25% quartile, respectively. The few outliers beyond the whiskers (vertical lines that extend to 1.5 times the upper and lower quartile) are plotted individually (+), and the arithmetic average of all 200 values is shown (\star).

Despite the large scatter in the individual measurements, the high repeatability and reproducibility of the measurement can be clearly seen from the evaluated parameters as for both, ionization rate coefficient and drift time, results overlap. The spread for both swarm parameters at higher pressures is smaller, because both the falling edge around T_e and the slope of the curve between T_1 and T_2 are steeper. For the ionization rate coefficient this effect is enhanced through the division by density N . The average drift time in between different sets of measurements varies by less than 0.5% and the average ionization rate by less than 3%. The evaluated average drift time at $p = 3$ kPa is 0.8 ns less than at $p = 10$ kPa. Using the measured drift velocities, this difference would correspond to a distance displacement of $\sim 100 \mu\text{m}$, but is hardly visible when comparing results on averaged waveforms. The accuracy of the distance was checked repeatedly and could hence be excluded as reason for this drift time difference. When normalized by density N , the effective ionization rate coefficient ν_{eff}/N for 3 kPa is 10% higher than at 10 kPa. The number of released electrons may vary during the measurement sequence due to aging of the photocathode or laser power fluctuations. With an increasing number of initial electrons, the measured displacement current increased, which seems to lead to a decreased scatter in the evaluated parameters. Nonetheless, the scatter in the average parameters seems to be unaffected by the varying scatter in the single measurement signals.

Besides single evaluated values, the most interesting one is the average value of swarm parameters. Different methods of averaging have been compared, A) applying the fit

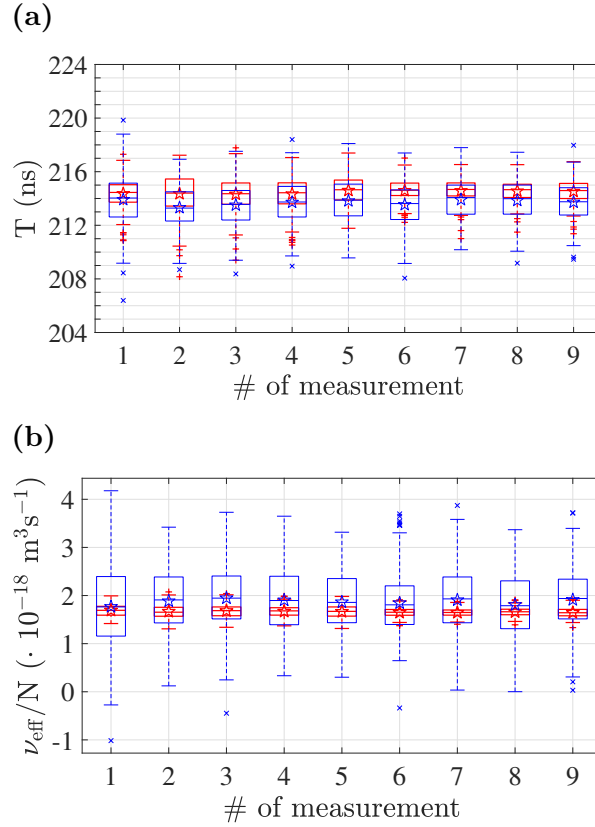


Figure 5: (a) Boxplots for 200 single evaluated drift times measured in N_2 at $(E/N) = 110 \text{ Td}$, $d = 25 \text{ mm}$ and $p = 3 \text{ kPa}$ (\square) and $p = 10 \text{ kPa}$, (\square). The same experimental setting was used 9 times per pressure. (\star) are average values of the evaluated single waveforms. (b) shows the boxplot and averages for the effective ionization rate coefficient for the same data set using the same color code as in (a).

(method described in section 3) on single waveforms and then averaging the swarm parameters. B) Averaging single waveforms on the oscilloscope and then applying the fit on averaged waveforms. C) The waveform is averaged afterwards on a computer. All methods generate similar results. For the drift time the deviations are in the range of the sampling frequency. In fig. 6 "regular" averaging is used. Whereas the focus is on repeatability of measurements in fig. 5, in fig. 6 the main aspect is the reproducibility. Hence, from data set 1) averages of different distances (13 and 25mm @ 10 kPa) and pressures (3 kPa and 10 kPa @ 25mm) are compared. As drift time changes with distance, only different pressures are compared. Unexpectedly, the uncertainty spread of drift times at 3 kPa and 10 kPa is smaller than the difference of the average between the measurements. For nitrogen, no pressure dependence has been reported, for neither the electron mobility, nor the ionization rate. Thus, it is investigated if the uncertainty of the average value is underestimated if taken from one set of measurements only.

For the drift time in fig. 6a a possible explanation of the differences could be due to

the limited bandwidth of the chamber and amplifier. From the amplifier manufacturer the transfer function was obtained. It was best approximated by a Butterworth filter of 3rd order. By inserting the obtained swarm parameter results in eq. (1) the measured waveform is compared to the theoretical model. Several effects such as noise and bandwidth limitation were added to the theoretical model to check their influence. These simulated waveforms are referenced as synthetic waveforms. The cutoff frequency of the Butterworth filter was determined by matching the rising edge of the synthetic waveform around T_0 to the measured averaged waveform. Hence, for the Butterworth filter a 3 dB cutoff frequency of 50 MHz was obtained. As this filter did not completely match other parts of the measured waveform, a first order low pass filter was implemented for comparison. A 3 dB cutoff frequency of 36 MHz was obtained. This is lower than the expected 70–80 MHz referenced in the manufacturers data sheet. As per the data sheet, a bandwidth of 36 MHz corresponds to a source capacitance of 70 pF which is above the calculated chamber capacitance. For measured waveforms changes in the gap distance showed a negligible influence, an indication that other capacitances are dominant.

Additionally, the evaluation method is applied to synthetically generated current traces, which are shown as well in fig. 6. The dashed line indicates the result from the direct evaluation of the synthetic curves. The drift velocity is independent of noise and hence not separately shown in the plot. The largest influence on the average evaluated drift time results when the signal is low-pass filtered with a 3 dB point at 36 MHz (green squares), which increases the drift time by ~ 1.5 ns. Low pressures with higher diffusion are less affected than higher pressures as additional simulations show. The use of a Butterworth filter reduces the drift time.

In contrast to this, the evaluation of the effective ionization rate is more influenced by noise: 3% of noise leads to a larger uncertainty and scatter ($\sim 3 \cdot 10^4 \text{s}^{-1}$). For single measured waveforms, the noise level corresponds more to 15%, which increases the uncertainty to $\sim 2 \cdot 10^5 \text{s}^{-1}$. The effective ionization rate coefficient is scaled by the number density N . The influence of 3% noise, low pass filter or Butterworth filter is negligible for the ionization rate coefficient.

Changes in the number of initial electrons, amplifier bandwidth limitations and changing capacitance with varying electrode distance are parameters which can limit the accuracy of the results. However, for the difference between high and low pressures there must be other influencing factors. This fact leads to the result that the repeatability of our setup is high. The reproducibility for different distances is high as the measurements for 13 and 25 mm in fig. 6b show. Although it slightly decreases for different pressures. The uncertainty given through the linear regression (effective ionization rate) and fit (drift time) are underestimated compared to the scatter of the individual measurements. Unfortunately, it is not possible to directly quantify this error and therefore the measurement error will continuously be used as an indicator for the resulting uncertainty. Qualitatively, one can state that the signal bandwidth is a sensitive parameter

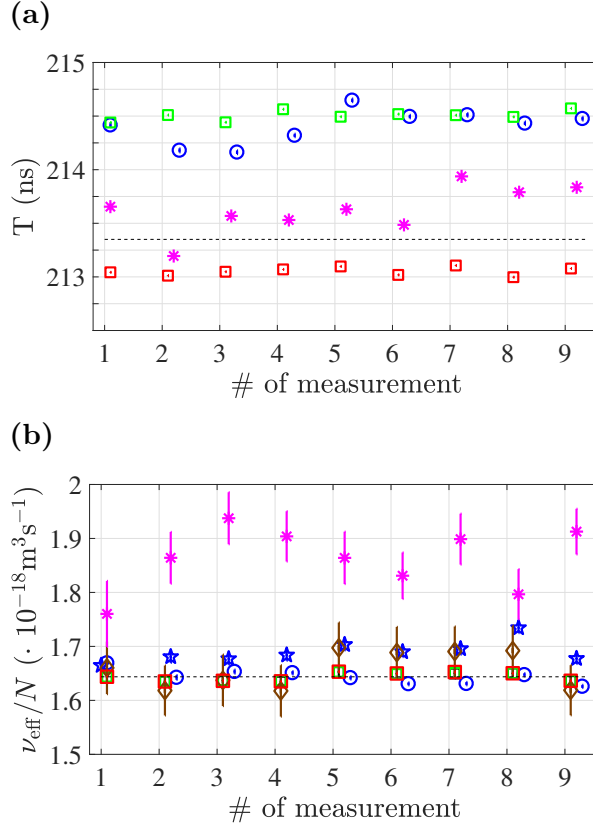


Figure 6: (a) Evaluated average drift times (*) 3 kPa and (o) 10 kPa both at 25 mm in N_2 . (----) initial value synthetic waveform for 10 kPa, (□) synthetic waveform with low pass filter 36 MHz, (□) synthetic waveform with Butterworth filter 50 MHz. (b) Ionization rates for measurements in N_2 . (o) 10 kPa at 25 mm and (★) 13 mm, (*) 3 kPa at 25 mm. Simulated results for $p = 10$ kPa are shown: (----) initial value synthetic waveform, fit of synthetic curve, 3% noise influence is not visible, (◇) synthetic curve with 15% noise and (□) synthetic curve with 3% noise and low-pass filter. (□) synthetic curve with 3% noise and Butterworth filter.

to determine the electron mobility (via drift time and influence on rising edge) and SNR for the scatter of the effective ionization rate.

An attempt to indirectly quantify the severity of the above mentioned influences on the scattering average values with varying experimental conditions is to compare them to an experimental error in (E/N) . Plotted in fig. 7a are the measured ν_{eff}/N values for nitrogen at $p = 3$ kPa, and at $p = 100$ kPa for lower (E/N) -values from data set 2). The two dashed lines correspond to the uncertainty of the measured curve, if the (E/N) -value would be wrong by $\pm 0.5\%$. In the zoom it is visible that the scatter of the measured average values is within those bounds in regions of increasing effective ionization rate coefficient (the region of main interest for us).

The second zoom in fig. 7b shows data set 1) and 2) combined. As the swarm

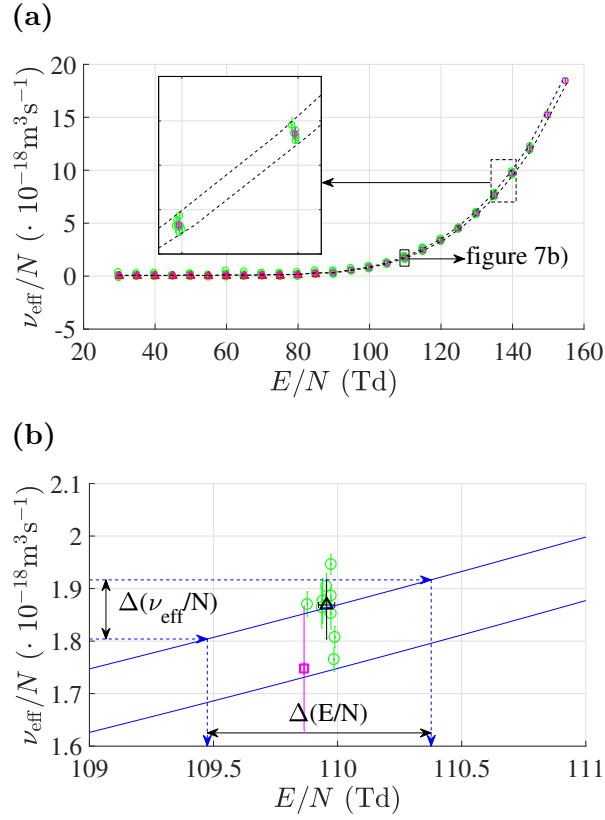


Figure 7: (a) Ionization rate coefficient measured at (\circ) 3 kPa and (\triangle) 100 kPa N_2 from data set 2), every circle or triangle is a different measured distance. For high (E/N)-values the individual ionization rate coefficients are within the dashed lines. The lines mark the limit which is $\pm 0.5\%$ from the average of all ionization rate points. (\square) are the average values of the 3 kPa measurements. (b) Sensitivity of fit checked by changing fit input parameters, 3 kPa N_2 at 25 mm from data set 1), (\triangle) median with 16 and 84 percentile of 9 times repeated measurements (\circ), (\square) are the average values of the 3 kPa measurements from data set 2).

parameter error of our model (section 3) might be underestimated, we analyzed the model sensitivity to its input parameters: I) instead of 200 single waveforms only 180 randomly selected waveforms were averaged. The decrease in SNR is negligible but the sensitivity of changes in the noise can be observed. II) and III) were a variation of the markers T_1 and T_2 in the range as they are applied in our evaluation. Each input parameter was changed 10 times so that in total one averaged waveform was evaluated 1000 times with different input sets of individual waveforms. The results seem to be normally distributed. Hence, the standard deviation for the error and the mean of the obtained value are plotted for data set 1) 3 kPa and 25 mm (\circ). This error is nearly identical to the one obtained from the linear regression and shown in fig. 6b. To obtain a distribution free result, the median of the 9 times repeated measurements (each composed of 200 individual waveforms) was calculated. The confidence interval

of the median value was calculated according to [19]. The error bars are the 16 and 84 percentile and are only slightly asymmetric, which means the distribution is nearly normal. Using the slope of the rate average obtained by data set 2), the error bar is projected on the x-axis. For the 75% confidence interval of the median value ($1.87 \cdot 10^{-18} \text{m}^3 \text{s}^{-1}$) is [1.853, 1.9048] the projection leads to $\Delta (E/N)$ of +0.13 Td and -0.14 Td in the worst case $\pm 0.13\%$. The difference of the 16 and 84 percentile is ± 0.52 Td which equals an error of $\pm 0.47\%$ at 110 Td which is higher than the theoretical approximation in section 4.1. The mean value at 110 Td for different distances has a higher spread of $\pm 0.8\%$. Regarding the median value of all distance measurements ($1.947 \cdot 10^{-18} \text{m}^3 \text{s}^{-1}$) the 95% confidence interval is [1.9058, 1.9811], which projects to $\Delta (E/N)$ of +0.27 Td and -0.33 Td in the worst case $\pm 0.3\%$. By including all distances, the confidence level for the median value could be increased to 95% compared to the median value of the repeated single distance measurements that only holds a confidence level of 75%. Even without being able to directly quantify the absolute measurement uncertainty, a comparison to literature data in section 4.3 clearly suggests that it is lower than in previous experiments.

Besides the above reported investigations, the following additional tests have been made to exclude their influence on the measurement uncertainty: long term stability of the motor positioning, amplifier bandwidth without electrode capacitance, and absence of influence of the laser repetition rate between 10-40 Hz.

4.3. Benchmark results

In figs. 8-11 the results for Ar, CO₂ and N₂ are compared to literature data, direct measurements and calculations (Bolsig+) / simulations (METHES) using electron scattering cross sections. Supplementary measurements at different pressures are published on LXCat [20]. Argon measurements were limited to 10 kPa due to strong ionization. Applying the methods presented in section 3, we obtain the effective ionization rate coefficient ν_{eff}/N , density normalized mobility μN and density normalized diffusion coefficient ND_L . In CO₂ ion currents are measured as well and we can separate the effective rate into an ionization and attachment rate constant. The different ion drift velocities are compared in CO₂ and N₂ to literature values. To compare our temporal swarm parameters to literature data, results are transformed to spatial swarm parameters as explained in section 3. The swarm parameter results for specific (E/N) -values are averages of measurement results at different distances as shown before with data set 2). The error bar is the standard deviation of these values, which could be seen as measure of the reproducibility for the measured distances, according to the introduced standard [2].

For calculations of Bolsig+ [21] version from 8/2012, and simulations of Methes [22] version from 06/2015 was used. Both simulation tools used the same cross section sets. For Ar a Phelps cross section set retrieved 2/2017, for CO₂ a Phelps cross section set retrieved 7/2014 and for N₂ a Siglo cross section set retrieved 12/2013 and a Biagi cross

section set retrieved 06/2015 from [23] were used. The swarm parameters, especially the ionization rate, showed a higher sensitivity to the used cross section set than the used simulation method. Nevertheless, cross section sets are not in the focus of this work but are rather used to demonstrate that there are differences between the available sets.

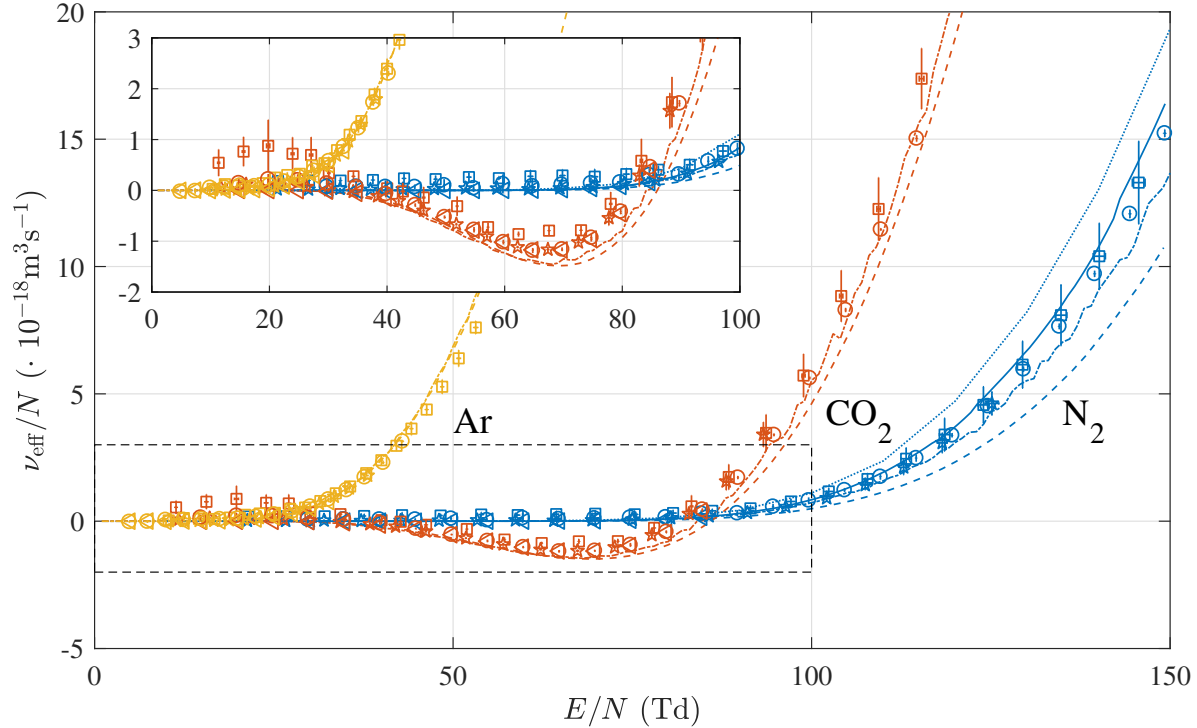


Figure 8: Effective ionization rate coefficient in Ar, N₂ and CO₂ versus (E/N) (\circ low pressure, \triangleleft high pressure) compared to measured values from our previous setup [8] (\square low pressure, \star high pressure) and to (---)N₂ Bolsig [21] using Siglo cross sections, (—) N₂ Bolsig using Biagi cross sections and (-·-) N₂ Methes [22] using Siglo cross sections, (·····) N₂ Methes using Biagi cross sections.

In fig.8 the effective ionization rate coefficient is shown. The chosen pressures are (3 k, 10 kPa) Ar, (3 k, 60 kPa) CO₂ and (3 k, 100 kPa) N₂ compared to [8] (3 k, 10.5 kPa) Ar, (3 k, 10.5 kPa) CO₂ and (3 k, 10.5 kPa) N₂. For the new results from this publication there was no need to correct the (E/N)-value, like it was done in the previous setup [8, 17]. Still for low (E/N)-values (e.g. < 25 Td for CO₂) there seems to be an abnormally high ionization rate, for CO₂ this effect is considerably lower compared to [8]. Overall our measurements agree better with the Monte-Carlo-Simulations from Methes for all gases. For N₂, our results are between Bolsig+ calculation with Biagi cross sections and Methes simulation with Siglo cross sections.

In fig. 9 the effective ionization coefficient is shown. As we provide a full set of swarm parameters, it is possible to scale our effective ionization rate constant with the corre-

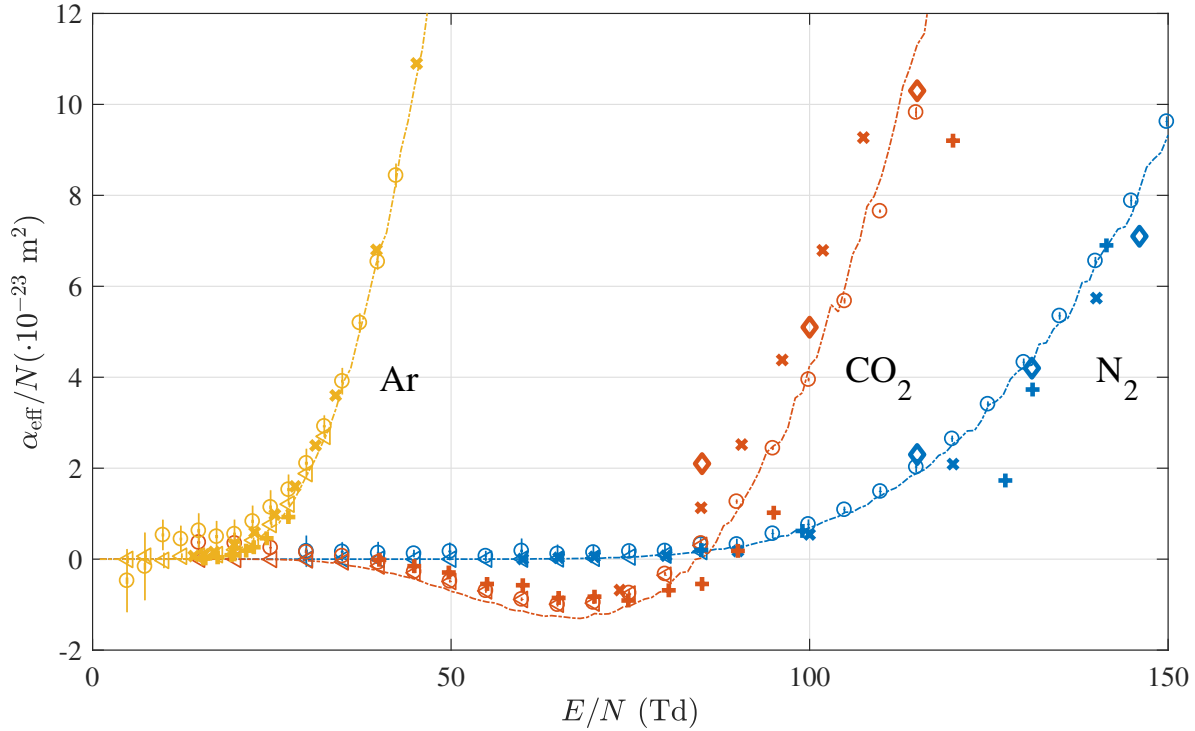


Figure 9: Effective ionization coefficient for Ar, N₂ and CO₂ (\circ low pressure, \triangleleft high pressure) compared to measured values from references and to Methes [22] (—). References for Ar are ($+$) Kruithof [24], (\times) Specht [25]), for CO₂ ($+$) Bhalla [26], (\times) Yousfi [27], (\diamond) Petri [5]) and for N₂ ($+$) Yousfi [27], (\times) Haydon [28], (\diamond) Petri [5])

sponding drift velocity and compare it to literature where only the effective ionization coefficient is given. The drift velocity increases for most measurements around a factor of 4. Hence, the ionization coefficient is like a zoom into the range of small ionization rates, which emphasizes the scatter around zero. This can be seen in low pressure measurements for Ar and CO₂. Our measurements for Ar agree well with the references from Kruithof [24] and Specht [25] over the whole measured range. For CO₂ our measurements are between those of Bhalla [26] and Yousfi [27], the spread in the values of reported ionization rate is quite significant in [27]. To quantify the spread, Bhalla obtained an ionization coefficient of $1.021 \cdot 10^{-23} \text{ m}^2$ at 95Td and Yousfi $\sim 4 \cdot 10^{-23} \text{ m}^2$. Yousfi's ionization rate coefficient was obtained by a linear interpolation between neighboring data points as his value was not exactly 95 Td. A good overall agreement to other experimental data is given for N₂. In [27] the scatter of the ionization coefficient seems to be higher, but this could be a digitization problem, as the data originates from a double logarithmic plot that was retrieved as number table from [29] 02/2017.

In fig.10 the density normalized electron mobility is shown. Bolsig calculations and Methes simulations agree very well for all gases over the whole (E/N)-range. For Ar our measurements apparently show a slight pressure dependence in the mobility, which

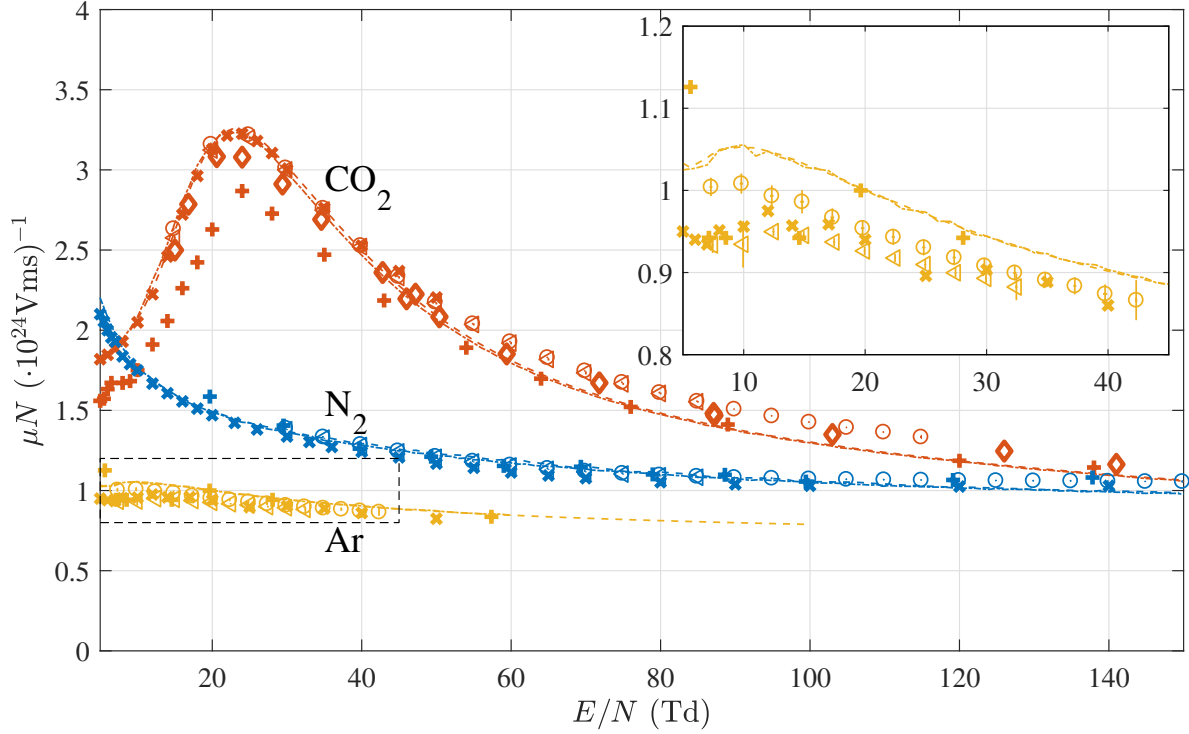


Figure 10: Density normalized electron mobility for Ar, N₂ and CO₂ (◦ low pressure, ◁ high pressure) compared to measured values from experimental references, Bolsig [21] (----) and Methes [22] (---). References for Ar are ((+)Nakamura [30], (x) Kucukarpaci [31]), for CO₂ ((+) Elford [32], (x) Yousfi [27], (◊) Vass [33]) and for N₂ ((+)Yousfi [27], (x) Hasegawa [34] by [35])

could be due to the bandwidth limitation difficulty as explained above (cf. section 4.2). Our measurements are between the simulations [21, 22] and measured values from [31]. Nakamuras [30] mobility is closer to the simulations. As visible in the zoom section of fig. 10, our low pressure measurements are closer to the simulation and the high pressure measurements agree quite well with the experimental reference from [31], for low (E/N)-values. At higher (E/N) the spread between the reference data itself and our data decreases. For the N₂ mobility experimental reference data itself, the simulations and our measurements agree very well over the whole (E/N) range. For CO₂, a maximum in the mobility around 20-30 Td can be observed. Our mobility agrees with the experimental data and the simulations. For higher (E/N)-values our mobility is slightly above the other references.

For the density normalized longitudinal diffusion coefficient shown in fig. 11, our measurements indicate a slight pressure dependency, which could, again, be due to the above mentioned bandwidth limitations. For higher pressures (above 10 kPa), the evaluation of ND_L is limited as D_L decreases and the fit results overestimate D_L . This can be seen in fig. 11 in the example of CO₂, where results for a pressure of 60 kPa (◻) are

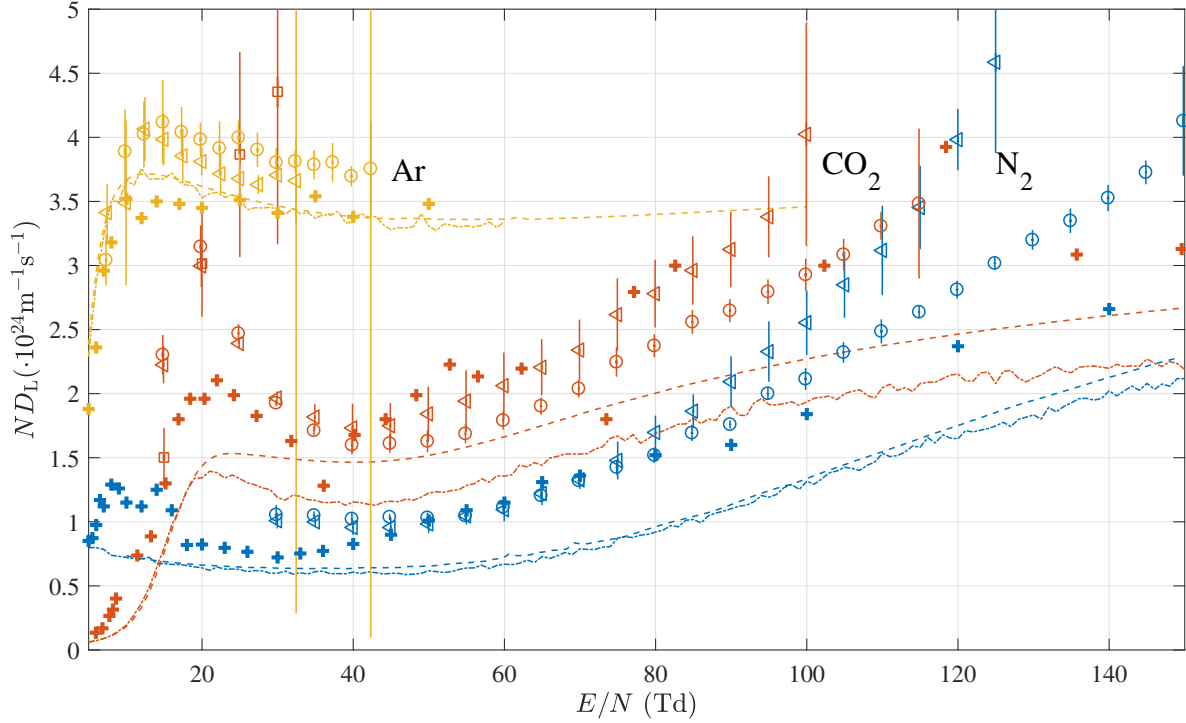
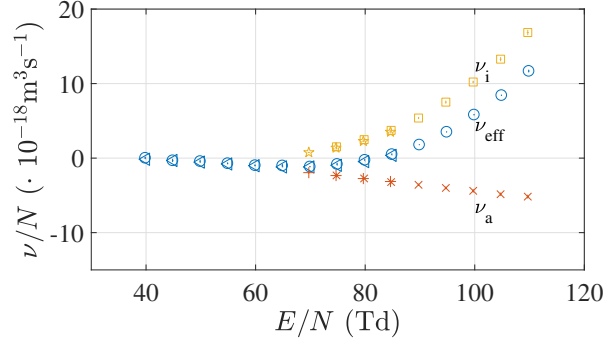


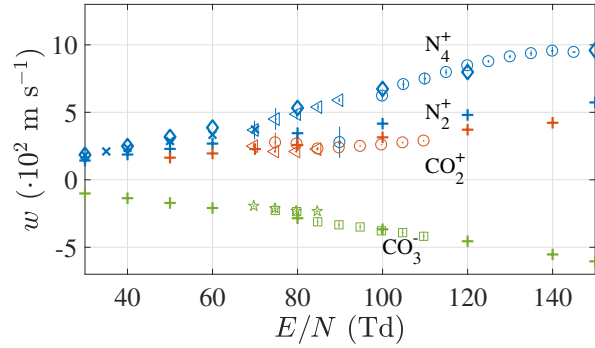
Figure 11: Density normalized longitudinal diffusion coefficient for Ar, N₂ and CO₂ (○ low pressure, ◻ high pressure, for CO₂ ◻) compared to measured values from references (+, x, ◊) and to Bolsig [21] (----) calculations and Methes [22] (—). References for Ar are (+) Nakamura [30]), for CO₂ (+) Yousfi [27]) and for N₂ (+) Yousfi [27])

shown as well, but the diffusion itself is too small to be evaluated. Already above 40 Td the results for 60 kPa are outside the selected diffusion constant range. Hence, for CO₂ 6 kPa and N₂ 10 kPa were selected. For all gases our results are above the simulation results. Due to experimental limitations, it is only possible to measure the smallest electrode separation distances at high pressures and high (E/N) values, which leads to a drastically increased error bar. Still, the error bars are added for completeness. ND_L for CO₂ and N₂ coincides with other experimental data over a wide (E/N)-range.

In fig. 12 the ion evaluation results for N₂ and CO₂ are displayed. As our experiment is not coupled to a mass spectrometer, we can only infer the type of ions by comparing them to literature values. Fig. 12a shows the ionization and attachment rate coefficients in CO₂ fitted according to eq. (4, 5). In fig. 12b obtained positive and negative ion drift velocities in N₂ and CO₂ including literature values are shown. For N₂ [38, 39, 40] suggests ionization leads to N₂⁺, which is converted to N₄⁺. The measured positive ion drift velocity agrees best with N₄⁺ for our measurement range. For CO₂ the positive drift velocity agrees very well with literature values from CO₂⁺ whereas negative ion drift velocities agree with CO₃⁻. As [41] suggests the O⁻ ions are converted to CO₃⁻ in our pressure and (E/N)-ranges. As the difference between positive and negative ion drift velocity CO₂ was very small, the negative ion drift velocity was scaled by (-1) for



(a)



(b)

Figure 12: (a) Ion current evaluation for CO_2 (a) ν_{eff}/N at different pressures (\circ 3 kPa, \triangleleft 60 kPa), ν_i/N (\square 3 kPa, \star 60 kPa) and ν_a/N (\times 3 kPa, $+$ 60 kPa). (b) ion drift velocities for CO_2 and N_2 at (3 kPa, 60 kPa) and measured values from other experiments ($+$, \times , \diamond). Measured drift velocity of positive ions in N_2 and CO_2 (\circ 60 kPa, \triangleleft 3 kPa) and negative ions in CO_2 (\square 60 kPa, \star 3 kPa) are scaled by (-1). References for N_2^+ in N_2 ($(+)$ Ellis [36], (\times) Viehland [37]), N_4^+ in N_2 (\diamond Ellis [36]), CO_2^+ in CO_2 ($(+)$ Viehland [37]) and ($+$) CO_3^- in CO_2 Ellis ([36])

better visibility. The ion reference data was digitized by [42, 43].

5. Discussion and Conclusion

This part highlights the implications of the design guidelines on the construction, chosen devices and their accuracy. Moreover, these implications are connected to the measurement results.

5.1. Design guidelines

Aim of the design was a filling pressure independent and highly accurate electrode separation adjustment, an increased electric field homogeneity over the whole electrode separation range, and a simplified handling of the gas filling and photocathode replacement. These requirements are fulfilled with the new concept and (E/N) -values can be

set with an accuracy of better than $\pm 0.5\%$ over a wide range of pressures, electrode separation and applied voltage. However, the design comes with an increased chamber volume.

In this experiment especially the reliable and accurate positioning of the electrodes is guaranteed by the locators and the high precision motor. The use of larger electrodes allowed us to increase the distance range to 35 mm without decreasing the homogeneity of the electric field. In our arrangement electric field distortions of protrusions were minimized through the use of photocathodes with a tailored support. Other concepts introduce inhomogeneities by using a mesh [10] to allow the laser light to reach the cathode. Through repeated measurements of the distance accuracy, other effects influencing the swarm parameter results can now be analyzed.

As the electric field could be influenced by space charge or excited species, it is important to check the laser intensity [44] and repetition rate. To ensure that prior pulses do not influence the following, the repetition rate was increased to its maximum of 40 Hz (requirement to operate the laser at stable power). All swarm parameters were compared, but no dependency is visible (i.e. smaller than the influence of the pressure itself). In other references the pulse repetition rate mostly remains unlisted. This is likely to be unproblematic, as the ion drift times are low compared to the repetition rate. Excited molecules are not likely to influence the results. Compared to [33], who uses a repetition rate of 3 kHz our rate is lower by orders of magnitude. Additionally, the power dissipated in the gas by [33] is higher, too.

The concept of [11] focuses on increasing the signal bandwidth, but comes at the expense of a lower electric field homogeneity and apparently affects the swarm parameters for gap distances larger than 10 mm. In our setup two options have been identified to decrease the total source capacitance: 1) the amplifier could be mounted closer to the anode, which increases the bandwidth theoretically to 105-170 MHz or 2) a cable optimized for low capacitance and vacuum is used in which the increase in bandwidth depends on its specifications. However, to exploit the full bandwidth of the used DHPCA-100, even further measures are necessary, which would lead to other trade-offs.

Another measurement setting uses the HCA-400M-5K amplifier with an ideal bandwidth of 400 MHz, at a source capacitance smaller than 5 pF. Comparing the rise time of waveforms measured by these amplifiers, no obvious difference becomes apparent. Hence, we conclude that the source capacitance is the main influence on the bandwidth limitations and both amplifiers are affected in a similar manner.

5.2. Averaging and error

Experimental noise influences the evaluation and can be decreased by signal averaging. This leads to a trade-off between noise reduction and total measurement time. In general, the accuracy of the effective ionization rate was mainly influenced by the SNR. Drift times and diffusion, however, are most influenced by the bandwidth limitation. For comparison: an uncertainty of 0.8 ns in evaluating the drift time (at our typical electron drift velocities) relates to an uncertainty in the electrode separation distance of $\sim 100 \mu\text{m}$. This is by factors larger than the actual accuracy that we can realize with our experiment.

The theoretical error of (E/N) can be compared to the experimental data as shown in fig. 7a. At high (E/N) already a small error in (E/N) can lead to a large error in the effective ionization rate. However, our measured rates are well within the limit. Therefore, our experimental data verifies the theoretical result of an accuracy of around $\pm 0.5\%$ in (E/N) . Further analysis of results for identical (E/N) but different experimental parameters U, d, p shows no systematic trend and all average values are within the mutual error bars. To conclude, the accuracy of this experiment is significantly increased compared to [8] and no regression method is required to correct the swarm parameters or (E/N) -values.

5.3. Summary and conclusion

A new Pulsed Townsend experiment to obtain swarm parameters was introduced in detail. Electron and ion currents are measured and evaluated. The main focus was to achieve a high accuracy in the (E/N) -values, which is a prerequisite to obtain precise swarm parameters. The highly precise and pressure independent electrode separation adjustment allowed to assess actual limitations of the experiment. The precision, repeatability and reproducibility were theoretically and experimentally verified. We presented a full set of consistent measurements for Ar, N_2 and CO_2 which were compared to our previous experiment, simulation results and literature data. The scatter within reference values from literature and in comparison to our measurements is in general larger than the reported (if reported at all) inaccuracies of the individual sets of measurements. The repeatability and precision in our measurements is very high, but the reproducibility was lower than the repeatability, especially for different pressures. We are aware that there is an influence of experimental parameters that cannot be avoided; namely the SNR and bandwidth limitations. We assume that other experiments suffer from similar difficulties and it cannot be ruled out that further, yet unknown, systematic errors lead to the deviations between different experiments. The remaining known errors in our experiment are mainly attributed to the bandwidth limitation and SNR, and future improvements addressing these two issues can be implemented on the experiment or evaluation method.

To further evaluate the accuracy of the resulting swarm parameters, a systematic study

using different measurement devices and theoretical evaluation routines is recommended.

Acknowledgments

This work is financially supported by GE Grid (Switzerland) GmbH, Pfiffner Technologie AG, ABB Switzerland and Siemens AG.

- [1] Nondestructive Testing resource center. Guide to the expression of uncertainty in measurements. <https://www.nde-ed.org/GeneralResources/ErrorAnalysis/UncertaintyTerms.htm>. Accessed: 2017-07-19.
- [2] Bureau International des Poids et Mesures. Guide to the expression of uncertainty in measurements. <http://www.bipm.org/en/publications/guides/gum.html>. Accessed: 2017-07-06.
- [3] Hyun-Ha Kim. Nonthermal plasma processing for air-pollution control: a historical review, current issues, and future prospects. *Plasma Processes and Polymers*, 1(2):91–110, 2004.
- [4] T Rößler, M Albert, R Terasa, and JW Bartha. Alternative etching gases to SF₆ for plasma enhanced chamber cleaning in silicon deposition systems. *Surface and Coatings Technology*, 200(1):552–555, 2005.
- [5] AR Petri, JAC Gonçalves, A Mangiarotti, S Botelho, and CC Bueno. Measurement of the first townsend ionization coefficient in a methane-based tissue-equivalent gas. *Nuclear Instruments and Methods in Physics Research Section A: Accelerators, Spectrometers, Detectors and Associated Equipment*, 2017.
- [6] P Camarri, R Cardarelli, A Di Ciaccio, and R Santonico. Streamer suppression with SF₆ in rpcs operated in avalanche mode. *Nuclear Instruments and Methods in Physics Research Section A: Accelerators, Spectrometers, Detectors and Associated Equipment*, 414(2):317–324, 1998.
- [7] LG Christophorou. Insulating gases. *Nuclear Instruments and Methods in Physics Research Section A: Accelerators, Spectrometers, Detectors and Associated Equipment*, 268(2-3):424–433, 1988.
- [8] Dominik A Dahl, Timm H Teich, and Christian M Franck. Obtaining precise electron swarm parameters from a pulsed townsend setup. *Journal of Physics D: Applied Physics*, 45(48):485201, 2012.
- [9] Heinz Raether. *Electron avalanches and breakdown in gases*. Butterworths, 1964.
- [10] J De Urquijo, CA Arriaga, C Cisneros, and I Alvarez. A time-resolved study of ionization, electron attachment and positive-ion drift in methane. *Journal of Physics D: Applied Physics*, 32(1):41, 1999.
- [11] H F A Verhaart and P. C T Van Der Laan. Fast current measurements for avalanche studies. *Journal of Applied Physics*, 53(3):1430–1436, 1982.
- [12] JM Wetzler, C Wen, and PCT van der Laan. Bandwidth limitations of gap current measurements. In *Electrical Insulation, 1988., Conference Record of the 1988 IEEE International Symposium on Electrical Insulation*, pages 355–358. IEEE, 1988.
- [13] P Haefliger and CM Franck. Assessing new SF₆ replacement gases through pulsed townsend experiments. *Int. Sympos. High Voltage Eng. (ISH)*, pages 24–28, 2014.
- [14] Manfred Beyer, Wolfram Boeck, Klaus Möller, and Walter Zaengl. *Hochspannungstechnik: theoretische und praktische Grundlagen*. Springer-Verlag, 2013.
- [15] K Siomos, J White, LG Christophorou, and JG Carter. Photoelectron injection in gases from thin metal films on quartz. *Chemical Physics Letters*, 63(3):584–590, 1979.
- [16] John M Meek and John Drummond Craggs. *Electrical breakdown of gases*. John Wiley & Sons, 1978.
- [17] A Chachereau, M Rabie, and CM Franck. Electron swarm parameters of the hydrofluoroolefine HFO1234ze. *Plasma Sources Science and Technology*, 25(4):045005, 2016.

- [18] A Hoesl, P Haefliger, and CM Franck. Measuring the pressure dependency of swarm parameters in dry air considering detachment and ion conversion. *Journal of Physics D: Applied Physics*, submitted.
- [19] Hanspeter Schmid and Alex Huber. Measuring a small number of samples, and the 3σ fallacy: Shedding light on confidence and error intervals. *IEEE Solid-State Circuits Magazine*, 6(2):52–58, 2014.
- [20] ETH database. Lxcat. <https://fr.lxcat.net/home/>. Accessed: 2017-02-21.
- [21] GJM Hagelaar and LC Pitchford. Solving the boltzmann equation to obtain electron transport coefficients and rate coefficients for fluid models. *Plasma Sources Science and Technology*, 14(4):722, 2005.
- [22] M Rabie and CM Franck. Methes: a monte carlo collision code for the simulation of electron transport in low temperature plasmas. *Computer Physics Communications*, 203:268–277, 2016.
- [23] LXCAt Database. Lxcat. <https://fr.lxcat.net/home/>. Accessed: 2017-02-21.
- [24] AA Kruithof. Townsend’s ionization coefficients for neon, argon, krypton and xenon. *Physica*, 7(6):519–540, 1940.
- [25] LT Specht, SA Lawton, and TA DeTemple. Electron ionization and excitation coefficients for argon, krypton, and xenon in the low E/N region. *Journal of Applied Physics*, 51(1):166–170, 1980.
- [26] MS Bhalla and JD Craggs. Measurement of ionization and attachment coefficients in carbon dioxide in uniform fields. *Proceedings of the Physical Society*, 76(3):369, 1960.
- [27] Mohammed Yousfi, Jaime de Urquijo, Antonio Juarez, Eduardo Basurto, and Jose Luis Hernandez-Avila. Electron swarm coefficients in CO₂-N₂ and CO₂-O₂ mixtures. *IEEE Transactions on Plasma Science*, 37(6):764–772, 2009.
- [28] SC Haydon and OM Williams. Combined spatial and temporal studies of ionization growth in nitrogen. *Journal of Physics D: Applied Physics*, 9(3):523, 1976.
- [29] UNAM database. Lxcat. <https://fr.lxcat.net/home/>. Accessed: 2017-02-21.
- [30] Y Nakamura and M Kurachi. Electron transport parameters in argon and its momentum transfer cross section. *Journal of Physics D: Applied Physics*, 21(5):718, 1988.
- [31] HN Kucukarpaci and J Lucas. Electron swarm parameters in argon and krypton. *Journal of Physics D: Applied Physics*, 14(11):2001, 1981.
- [32] MT Elford and GN Haddad. The drift velocity of electrons in carbon dioxide at temperatures between 193 and 573 k. *Australian Journal of Physics*, 33(3):517–530, 1980.
- [33] M Vass, I Korolov, D Loffhagen, N Pinhao, and Z Donko. Electron transport parameters in CO₂: scanning drift tube measurements and kinetic computations. *arXiv preprint arXiv:1611.07447*, 2016.
- [34] H Hasegawa, H Date, M Shimozuma, K Yoshida, and H Tagashira. The drift velocity and longitudinal diffusion coefficient of electrons in nitrogen and carbon dioxide from 20 to 1000 Td. *Journal of Physics D: Applied Physics*, 29(10):2664, 1996.
- [35] Laplace database. Lxcat. <https://fr.lxcat.net/home/>. Accessed: 2017-02-21.
- [36] HW Ellis, RY Pai, EW McDaniel, EA Mason, and LA Viehland. Transport properties of gaseous ions over a wide energy range. *Atomic Data and Nuclear Data Tables*, 17(3):177–210, 1976.
- [37] LA Viehland and EA Mason. Transport properties of gaseous ions over a wide energy range, iv. *Atomic Data and Nuclear Data Tables*, 60(1):37–95, 1995.
- [38] Mario Capitelli, Carlos M Ferreira, Boris F Gordiets, and Alexey I Osipov. *Plasma kinetics in atmospheric gases*, volume 31. Springer Science & Business Media, 2013.
- [39] M Saporoschenko. Mobility of mass-analyzed N⁺, N₂⁺, N₃⁺, and N₄⁺ ions in nitrogen gas. *Physical Review*, 139(2A):A352, 1965.
- [40] RN Varney. Equilibrium constant and rates for the reversible reaction N₄⁺, N₂⁺⁺, N₂. *Physical Review*, 174(1):165, 1968.
- [41] TD Fansler, LM Colonna-Romano, and RN Varney. Negative ions in CO₂. *The Journal of Chemical Physics*, 66(7):3246–3251, 1977.

- [42] Viehland database. Lxcat. <https://fr.lxcat.net/home/>. Accessed: 2017-04-30.
- [43] Phelps database. Lxcat. <https://fr.lxcat.net/home/>. Accessed: 2017-04-30.
- [44] CM Franck, DA Dahl, M Rabie, P Haefliger, and M Koch. An efficient procedure to identify and quantify new molecules for insulating gas mixtures. *Contributions to Plasma Physics*, 54(1):3–13, 2014.